RESEARCH PAPER

Mechanical Degradation of Reinforced Concrete Columns Corroded Under Sustained Loads

Qiang Li[1] · Le Huang[2] · Hailong Ye[2] · Chuanqing Fu[3] · Xianyu Jin[4]

Abstract

This study presented an experimental investigation on the degradation of mechanical performance of reinforced concrete (RC) columns with the reinforcements corroded under sustained loads. A total of ten RC column specimens were tested. The effects of different levels of sustained load (0%, 30%, and 60% of the designed ultimate bearing capacity N_u) and reinforcement corrosion (0%, 5%, 10%, and 20%) on the failure modes, ultimate bearing capacity, and axial load–axial deformation relationship were analyzed. The results showed that the coupling adverse effects due to the reinforcement corrosion and sustained load considerably exacerbate the mechanical deterioration of RC columns and turn the failure mode into a much more brittle manner. Compared with the control specimen L-0-0, the ultimate bearing capacity of the specimen L-4-20 could be reduced as much as about 42%. Based on the test results, an improved model was proposed to estimate the ultimate bearing capacity of corroded RC columns, in which the effects of the corrosion of both longitudinal reinforcements and stirrups and the corrosion-induced spalling of concrete cover were taken into consideration. The close agreements between the analytical predictions and test results prove the applicability of the model.

1 Introduction

✉ Hailong Ye
   hlye@hku.hk

   Qiang Li
   liq@zjweu.edu.cn

   Le Huang
   Huangle@hku.hk

   Chuanqing Fu
   chqfu@zju.edu.cn

   Xianyu Jin
   xianyu@zju.edu.cn

1   College of Civil Engineering and Architecture, Zhejiang University of Water Resources and Electric Power, Hangzhou, China

2   Department of Civil Engineering, The University of Hong Kong, Pokfulam, Hong Kong, China

3   College of Civil Engineering and Architecture, Zhejiang University of Technology, Hangzhou, China

4   College of Civil Engineering and Architecture, Zhejiang University, Hangzhou, China

In practice, deterioration of columns often results in a high risk of the collapse of reinforced concrete (RC) structures, for the reason that as one of the paramount structural members, the columns almost support all of the vertical loads, as well as some frequent lateral loads [1]. Thus, the performance of columns under various loading and environmental conditions has always been one of the major concerns during the whole service life [2–5]. To date, the crucial parameters that affect the mechanical properties of RC columns have been well understood and documented, and important among these factors include the concrete strength, thickness of concrete cover, axial compression ratio, and slenderness [6–8]. However, existing studies have shown that in the case of harsh environments, considerable degradations of the mechanical properties of RC columns, in terms of the ultimate bearing capacity, ductility, dynamic responses, etc., are still generally observed due to the reinforcement corrosion and concrete spalling,

although the protection measures are satisfied with the requirements of design codes [9, 10].

To tackle this issue, a large number of investigations on the mechanical behavior of corroded RC columns have already been conducted, and many referential results have been obtained. Some researchers [11–13] experimentally studied the stiffness, ductility, and ultimate bearing capacity of the corroded reinforced concrete columns. The results showed that for corroded RC columns, the causes for the decline of mechanical properties of an RC column are mainly due to the loss of the bond, reduction in confining effects of concrete, and especially the performance degradation of steel reinforcements. As such, the influences of reinforcement corrosion on the mechanical behaviors of RC columns were analyzed in [14, 15]. Upon the accelerated corrosion approach, some other researchers studied the performance of RC columns with partial reinforcement corrosion, in which the parameters of corrosion length and stress state were emphatically discussed [16, 17]. Similar contributions can also be found in the literature [18–20]. Nevertheless, it is noted that for the majority of the above studies, only the corrosion of the longitudinal reinforcement is taken into consideration, which, however, is quite not consistent with the actual situations where both the longitudinal reinforcements and stirrups are observed to corrode, and sometimes the stirrups are even subjected to a more serious corrosion because of the thinner concrete cover [21].

On the other hand, considering the actual stress state of columns, some efforts have also been dedicated to introduce the effects of external service loads into the analyses of the mechanical performance of corroded RC members [22–24]. The degradation laws of the mechanical performance of RC columns along with the continuous corrosion of longitudinal reinforcements were investigated in [25]. However, in this study, only the situation of axial compression on the columns was analyzed. Besides, an experimental research on the RC columns subjected to eccentric load was also carried out, followed by an alternation of the dry–wet environment [26]. Other scenarios like the freeze–thaw alternation, high-low temperature cycling, etc., have also been discussed together with various types of loads [27–29]. For most of the above research, the environmental influences and sustained load, however, are not considered simultaneously, but in different stages. Thus, the coupling effects of these two parameters on the mechanical performance of corroded RC columns remain unclear.

To fill the above-mentioned research gaps, this paper aims to study the mechanical properties of RC columns with reinforcement corrosion along with sustained loads. As such, the potential acceleration effect of external loads on the corrosion development of RC columns can be observed. The failure modes, cracking patterns, and load–axial deformation relationship of the RC columns corroded under sustained loads are analyzed. Based on the test results, an improved model is proposed to estimate the ultimate bearing capacity of corroded RC columns, in which the effects of the corrosion of both longitudinal reinforcements and stirrups, as well as the concrete spalling, are taken into consideration.

2 Experimental Program

2.1 Material Properties

In accordance with the specification JGJ 55-2011 [30], the proportion of the mix was designed as cement: water/sand/coarse aggregate = 1: 0.53: 2: 3 (by mass). Ordinary Portland cement P.O 52.5 from Huber Hoaxing Plant was used as the binder. River sand was used as the fine aggregate, and continuous graded crushed limestone with 5–20 mm was used as coarse aggregate. The 28-day compressive strength of the concrete cubes (150 mm × 150 mm × 150 mm) was measured to be 29.47 MPa.

For steel reinforcements, both the longitudinal reinforcements and the stirrups were HPB235 plain bar, whose mechanical properties are listed in Table 1.

2.2 Specimens Preparation

In order to investigate the coupling effects of reinforcement corrosion and sustained load on the mechanical performance of RC columns, a total of ten specimens with an identical dimension of 120 mm × 120 mm × 750 mm were designed, as shown in Fig. 1.

Table 1 Mechanical properties of steel reinforcements

	Nominal diameter (mm)	Elastic modulus (GPa)	Yielding strength (MPa)	Ultimate strength (MPa)	Elongation (%)
Longitudinal reinforcements	10	184	333.2	477.9	25.8
Stirrups	6	205	421.1	553.9	18.9
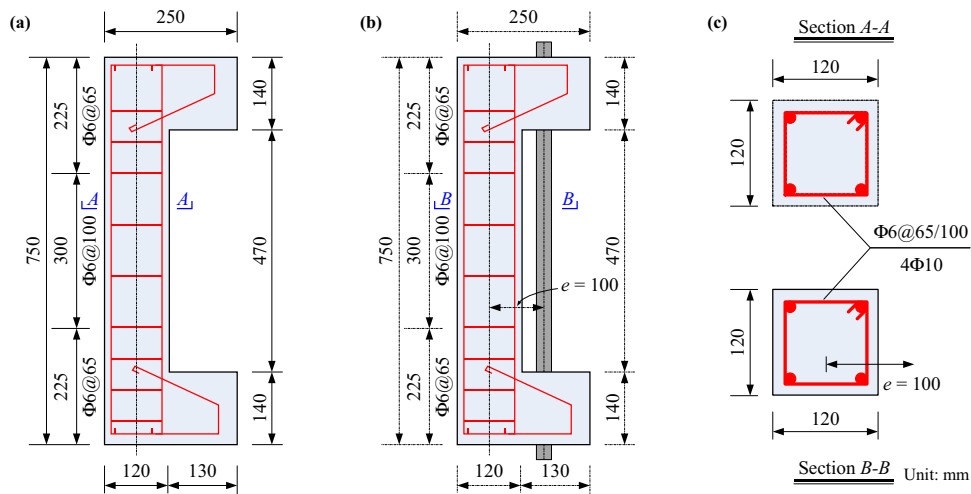
Fig. 1 Configuration of specimens. **a** Control specimen, **b** other specimens, **c** cross section of specimens

With the motivation to represent the actual stress state of RC columns in service, the typical scenario of eccentrically loading was considered in this study. For better application of such an eccentric sustained load, two additional corbels were specially designed at the ends of each column where the stirrups were spaced closer (65 mm apart) to prevent potential local failure. Besides, a screw-thread steel bar was mounted away from the geometric center with a distance of 100 mm. Four steel plain bars with a diameter of 10 mm were used as the longitudinal reinforcements, and the thickness of concrete cover was uniformly fixed at 15 mm. To simulate the service loads, two load levels, i.e., 30% and 60% of the designed ultimate bearing capacity, were selected in this study. The details of the specimens are shown in Table 2.

2.3 Implementation of Sustained Load

To apply the sustained load, the so-called self-balancing prestressing method illustrated in Fig. 2 was adopted. The sustained load was implemented as long as the 28-day strength of the specimens was achieved. Upon the pressure generated from the oil pump, the screw-thread steel bars were firstly tensioned, which would then exert compression on the specimens in turn when the prestress was fixed, as shown in Fig. 3. To ensure that the sustained load being maintained to the targeted level, periodical examinations were performed to compensate for the possible stress relaxation.
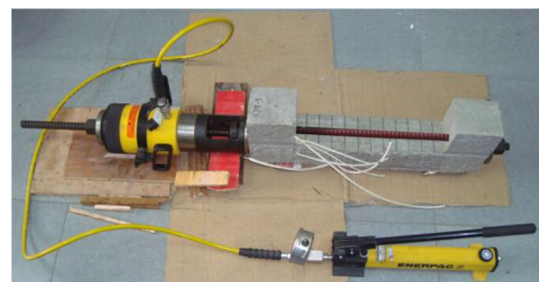
2.4 Accelerate Corrosion

The electrochemical method (impress current method) was used to accelerate the corrosion of reinforcements, as

Table 2 Details of the specimens

Column	Load ratio	Designed load (kN)	Actual load (kN)	Corrosion level (%)
LC-0-0	0	0	0	0
LC-0-5	0	0	0	5
LC-0-10	0	0	0	10
LC-0-20	0	0	0	20
LC-2-5	30	19.2	20	5
LC-2-10	30	19.2	20	10
LC-2-20	30	19.2	20	20
LC-4-5	60	38.5	40	5
LC-4-10	60	38.5	40	10
LC-4-20	60	38.5	40	20

The nomenclature of specimen is LC-*a*-*b*, where *a* and *b* represent the load level and the corrosion level, respectively. For example, LC-4-5 represents the column that is subjected to a sustained load of 40 kN, accompanied by an expected reinforcement corrosion level of 5%

Fig. 2 Prestressing process

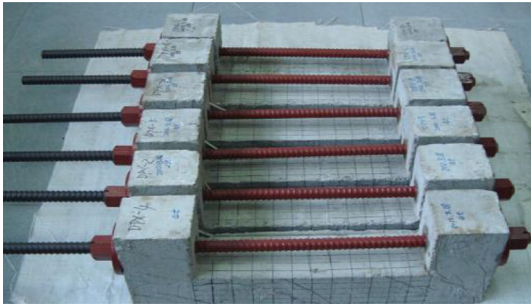shown in Fig. 4. The surfaces of the specimens were wrapped with a wet sponge and a stainless steel cage
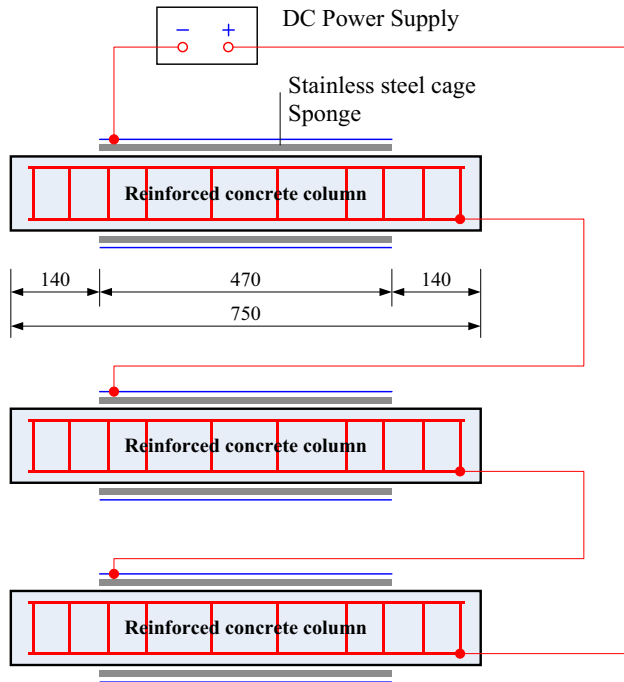
Fig. 3 Preloaded specimens

Table 3 Designed duration of the corrosion process

Corrosion level (%)	Mass loss (g)	Current density (A/cm²)	Cross-sectional area (cm²)	Current (A)	Corrosion time (h)
5	97.6	0.0002	1238.42	0.248	377.24
10	195.2	0.0002	1238.42	0.248	754.48
20	390.4	0.0002	1238.42	0.248	1508.36

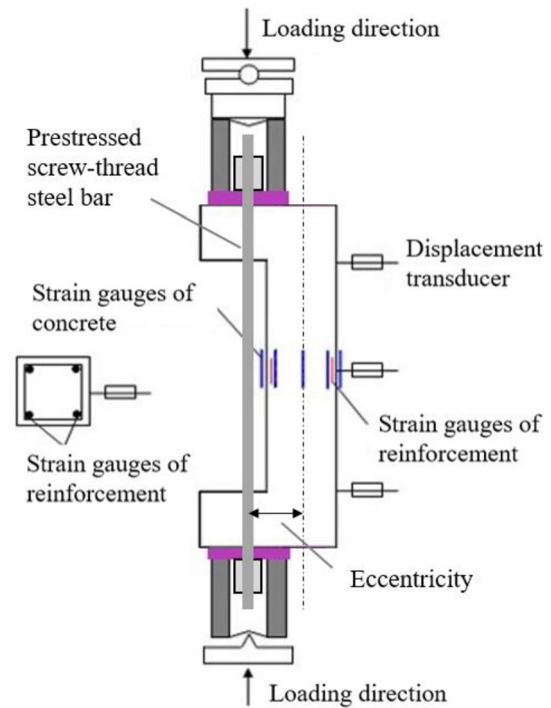**Fig. 4** Setup of the accelerate corrosion

Fig. 5 Schematic diagram of the eccentric loading

2.5 Loading Test

The test setup is illustrated in Fig. 5, in which the preloaded RC columns were further eccentrically loaded at the same location of the prestress. For each specimen, three displacement transducers were mounted on the bending side to measure the lateral deflection. Besides, to record the development of the cross-sectional deformation within the specimens, five strain gauges were arranged to monitor the strain changes of the concrete surface. Two of them were glued to the tension and compression sides, respectively, while the rest three were parallelly glued to the lateral side of the specimens.

The specimens were tested immediately when the targeted durations of corrosion process were achieved. In the beginning, a preloading procedure was firstly performed to ensure all the components being touched closely. After that, a predetermined axial loading procedure was carried out as follows: Before reaching the cracking strength, the

successively. To prevent the occurrence of the anchoring members been destroyed, the embedded reinforcements were covered with epoxy resin at both ends with a length of 120 mm, and the actual corrosion length, therefore, was 470 mm. Finally, the reinforcements and the stainless steel cage wire were connected to a power supply. In this system, the reinforcements served as the anode, while the stainless steel wire served as the cathode.

According to Faraday's law, the duration of the corrosion process of each specimen was calculated and is shown in Table 3. It should be noted that except for the control specimens, for all the other specimens, during the whole corrosion process, as well as the subsequent axial loading stage, the sustained loads were always maintained.

increment in load at each step was less than 20% of the failure load, which was then reduced to 10% of the failure load when approaching the cracking strength. The loading interval was not less than 15 min.

The test stopped when the maximum bearing capacity of the specimen was reached. During the whole test, the values of the applied load, lateral deflection, concrete strain, and evolution of cracks were recorded simultaneously.

2.6 Determination of Corrosion Level

After the loading test, the reinforcement cages were taken out from the broken columns. Following the specifications in GB/T 50082-2009 [31], the corrosion products of reinforcements were removed by mechanical and chemical cleaning, followed by a full drying. As a consequence, the reinforcement corrosion level of each specimen was quantitatively determined by comparing the difference in mass between the original and final states.

3 Results and Discussion

3.1 Failure Characteristics

An overall view of the failure modes of specimens under the axial load is illustrated in Fig. 6. The results showed

that the sustained load and reinforcement corrosion have obvious coupling effects. For all specimens, during the test, the longitudinal reinforcements far away from the side of the axial load first reached the tensile yielding strength, followed by the crush of the concrete close to the axial load, accompanied by the transverse cracks formed in the tension zone. With the increase in axial load, the tensile reinforcement entered into the flow stage, and the transverse cracks in the tension zone gradually extended to the compression zone, resulting in a decrease in the height of the compression zone of concrete. Finally, the edge of the concrete in the compression zone reached the ultimate compressive strain, and longitudinal cracks appeared in this zone.

3.2 Reinforcement Corrosion Level

The measured actual corrosion levels of all specimens are shown in Fig. 7. From Fig. 7a, b, it can be seen clearly that in general, the corrosion level of stirrups is higher than that of longitudinal reinforcements, correspondingly. Three main reasons are deemed to account for this observation. First of all, compared with the longitudinal reinforcements, the concrete cover of stirrups is relatively smaller, providing easier access to the higher concentration of chloride ions. Secondly, due to the fact that the diameter of longitudinal reinforcements is larger than that of stirrups, the current density within the stirrups, therefore, is bigger, in
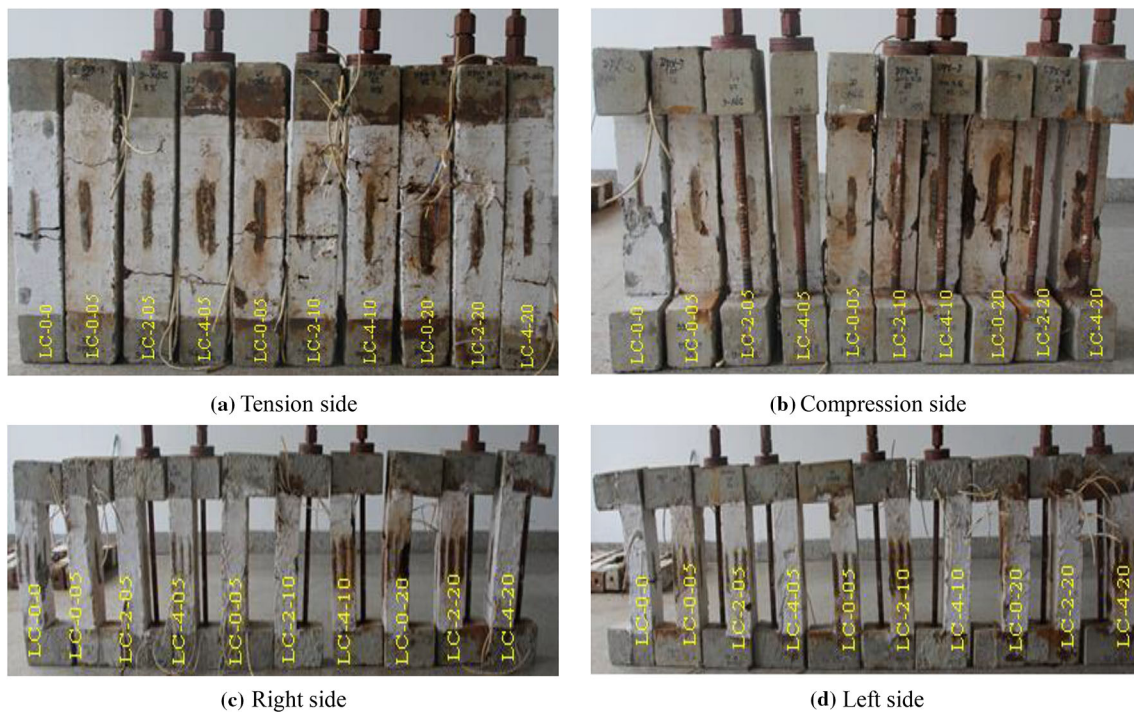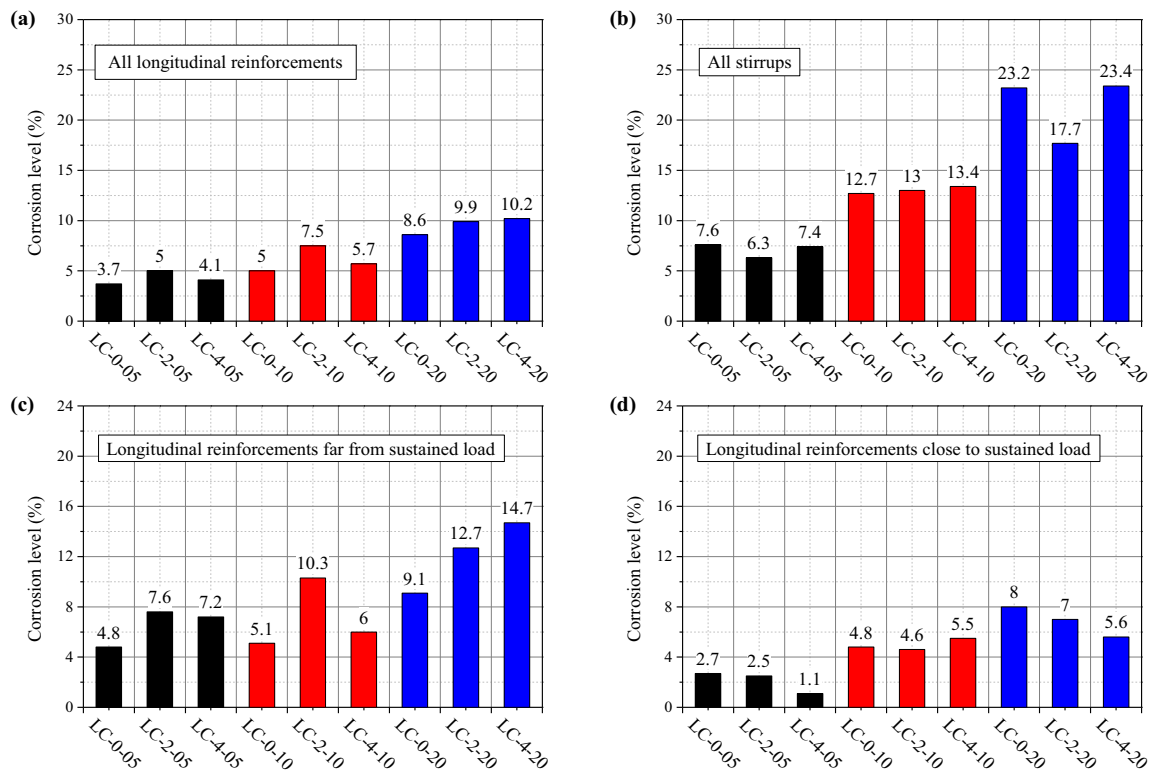
(a) Tension side

(b) Compression side

(c) Right side

(d) Left side

Fig. 6 Failure modes of RC columns

Fig. 7 Measured corrosion levels of specimens

the case of the same current flows through. This also exacerbates the corrosion of stirrups, according to Faraday's law that the corrosion level is proportional to the current density. Last, in practice, the corrosion potential of stirrups is higher, which actually plays galvanic protection to the longitudinal reinforcements.

Furthermore, for the corrosion level of longitudinal reinforcements, the comparison between Fig. 7c, d indicates that the sustained load has an obvious effect on it. More specifically, the corrosion level of reinforcements on the side far from the sustained load is apparently greater than that on the side closer to the sustained load, and this observation becomes much more pronounced as the load level increases. This is attributed to that under sustained load, more tension cracks may be formed on the side far from the load, which in turn promotes the ingress of chloride ions to the surface of steel reinforcements.

3.3 Distribution of Corrosion-Induced Cracks

The distribution of corrosion-induced cracks on the surfaces of all specimens is exhibited in Fig. 8. From the comparisons, it is clear that as the corrosion level increases, the number of cracks, as well as the crack width, increases gradually, and more corrosion products leak out from the inner concrete. For each specimen, it is also observed that the leakage of rust on the side far from the sustained load is

more than that near the sustained load. This further indicates that the sustained load has an obvious effect on reinforcement corrosion, which is consistent with the measured results of the reinforcement corrosion level mentioned above.

Moreover, as shown in Fig. 8, it also can be seen that the expansions induced by the rust from stirrups and longitudinal reinforcements, respectively, are quite different. That is, the corrosion of stirrup generally results in a local bulge and spalling of concrete cover where the stirrups located, while the corrosion of longitudinal reinforcements usually forms some cracks along the steel bars. This observation is mainly caused by the thicker concrete cover of longitudinal reinforcements, whose corrosion-induced expansion is further restrained by stirrups.
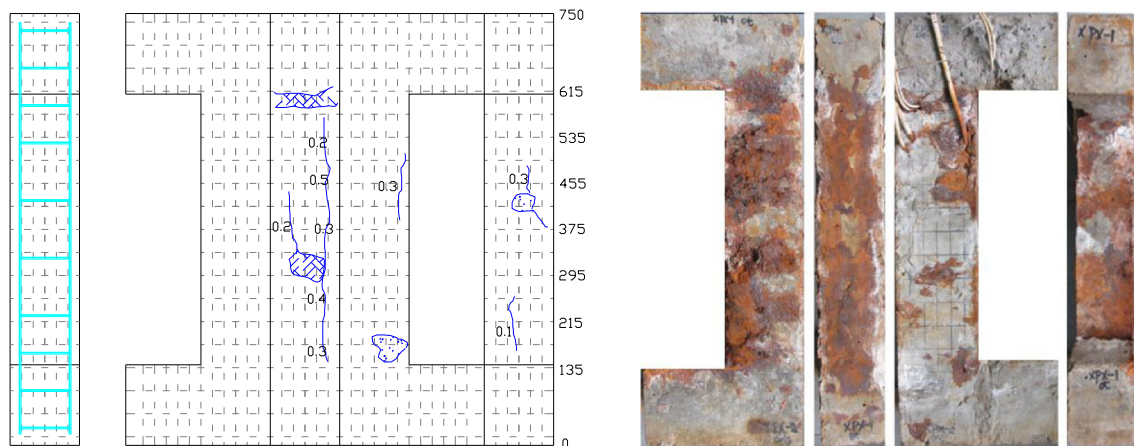
3.4 Load–Axial Displacement Responses

The load–axial displacement responses of specimens are plotted in Fig. 9. The effects of corrosion level and sustained load on the axial compressive performance were analyzed.
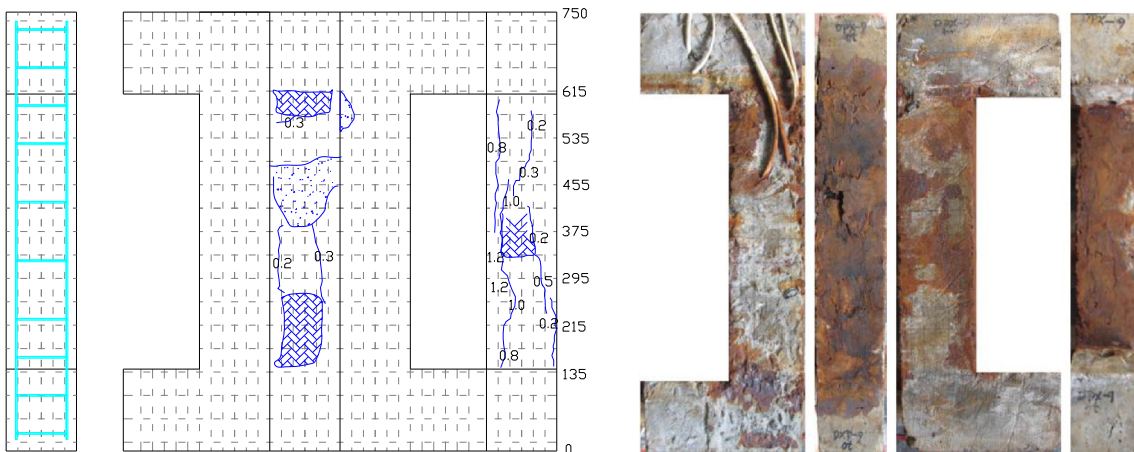
The load–axial displacement curves of the large eccentric columns with the same sustained load but different corrosion levels are shown in Fig. 9a–c. From the comparisons, it can be seen that the axial ultimate displacement of the corroded column is smaller than that of non-corroded
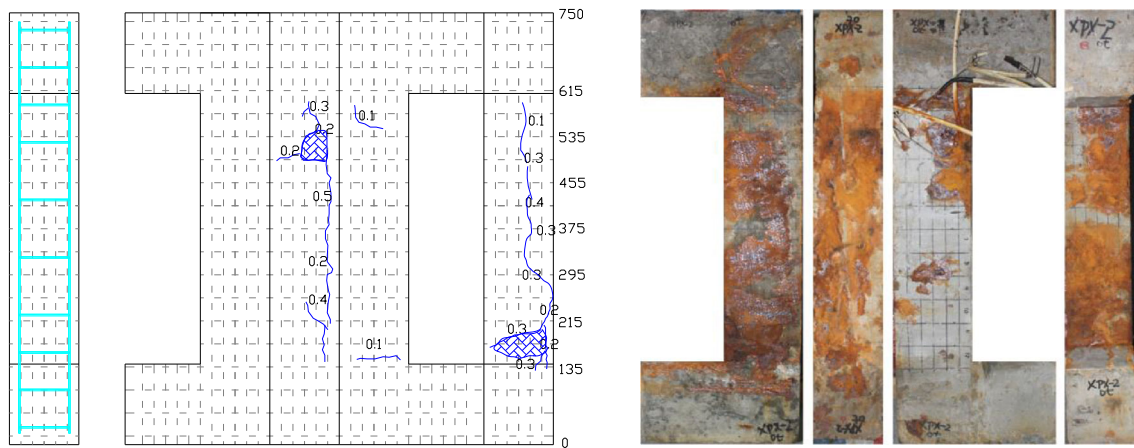
(a) LC-0-05

(b) LC-0-10

(c) LC-0-20

**Fig. 8** Reinforcement corrosion-induced cracking of specimens

columns, and as the increase in corrosion level, the ultimate displacement of corroded columns decreases gradually. Moreover, the slope of load–axial displacement curves of corroded columns is smaller than that of non-corroded one, implying a smaller stiffness. This indicates that the brittle nature of columns becomes more pronounced as the increase in the corrosion level.
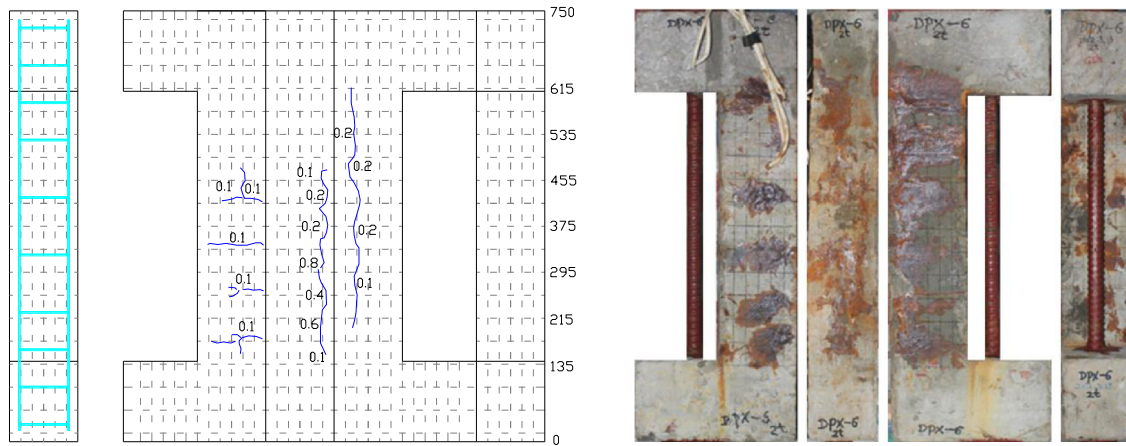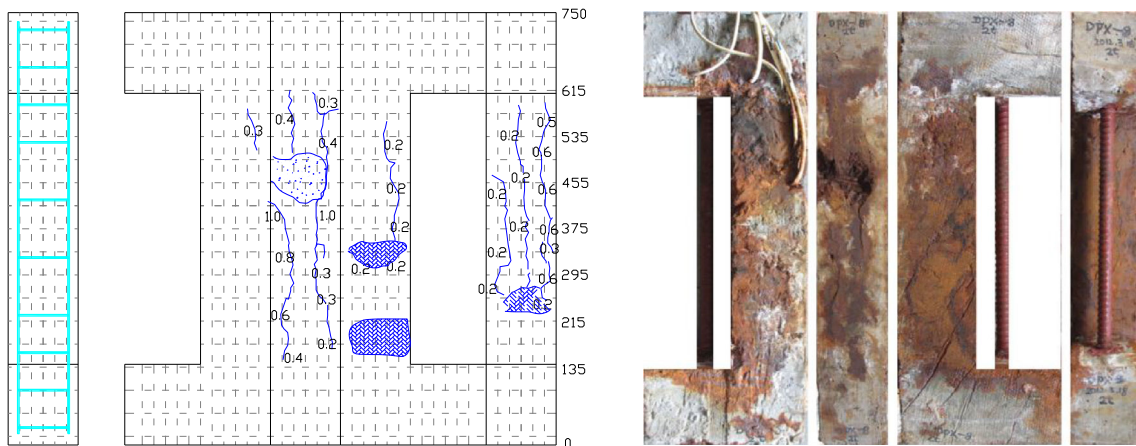
(d) LC-2-05
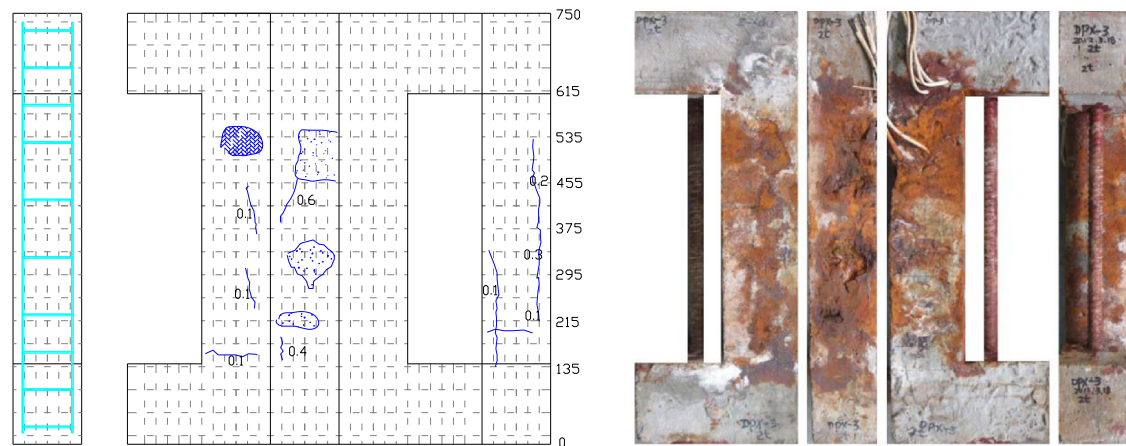
(e) LC-2-10


(f) LC-2-20

Fig. 8 continued

Likewise, the load–axial displacement curves of the large eccentric columns with the same corrosion level but different sustained loads are shown in Fig. 9d–f. It can be generally seen that in most cases, the slopes of load–axial displacement curves of the columns without the sustained load are smaller than those with sustained loads, indicating
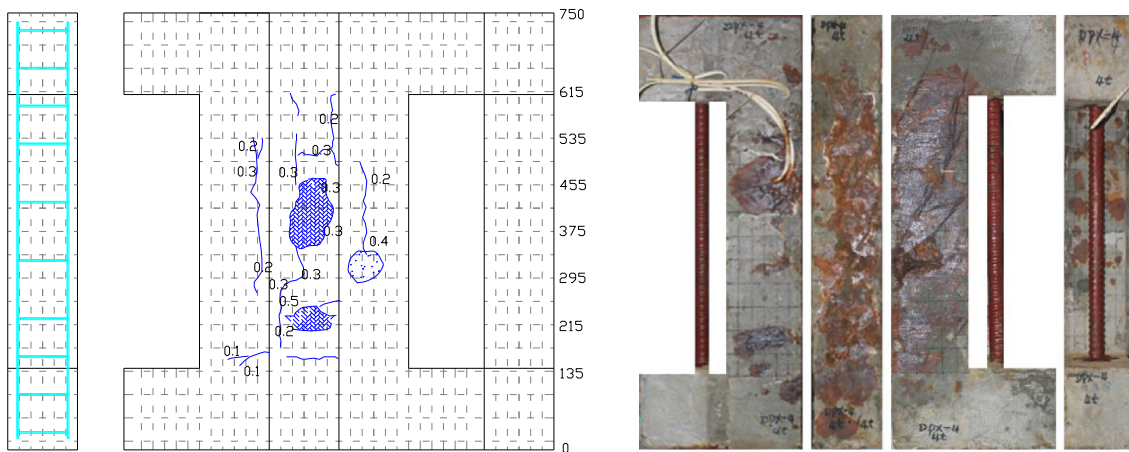
(g) LC-4-05
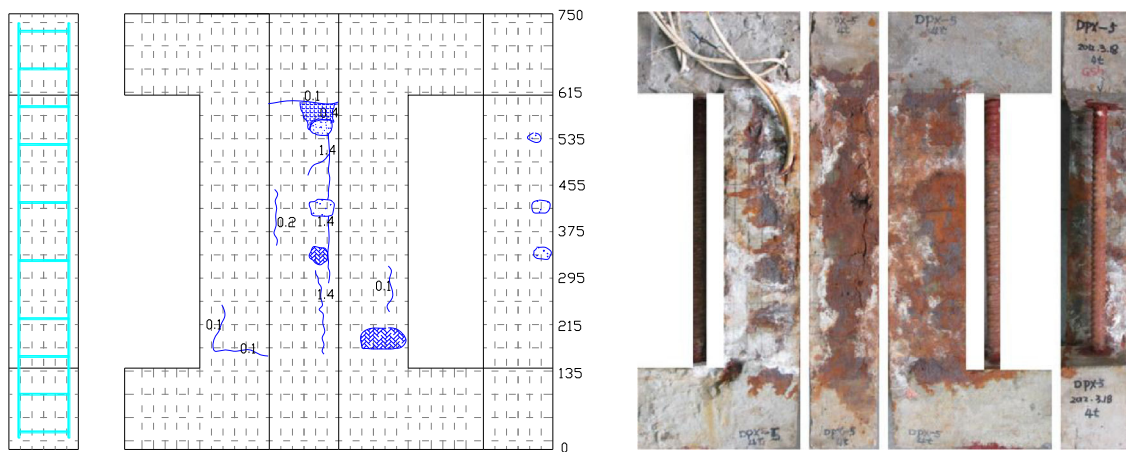
(h) LC-4-10

(i) LC-4-20

Fig. 8 continued

the stiffness of columns with the sustained load seems to be enhanced. However, on the other hand, the poorer ductility indicates that the sustained load exacerbates the brittle failure of specimens.

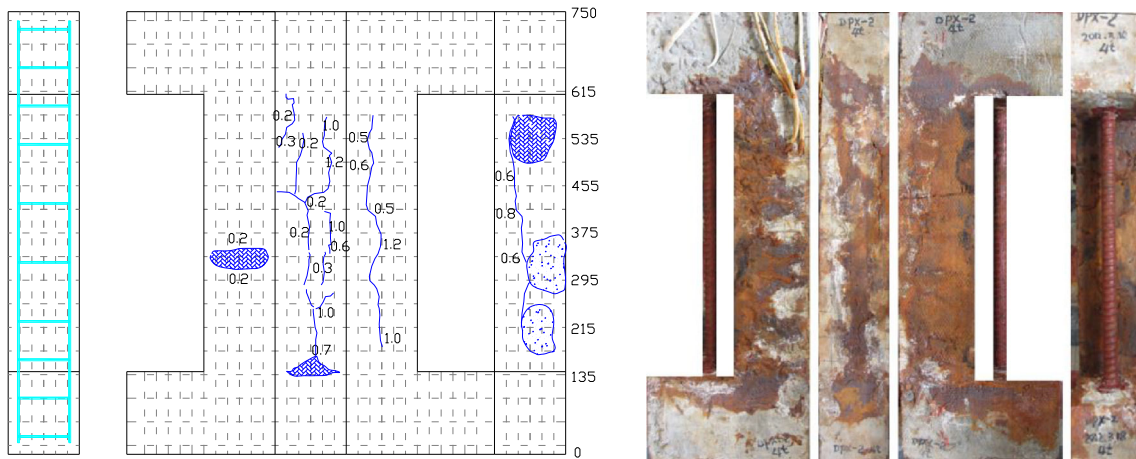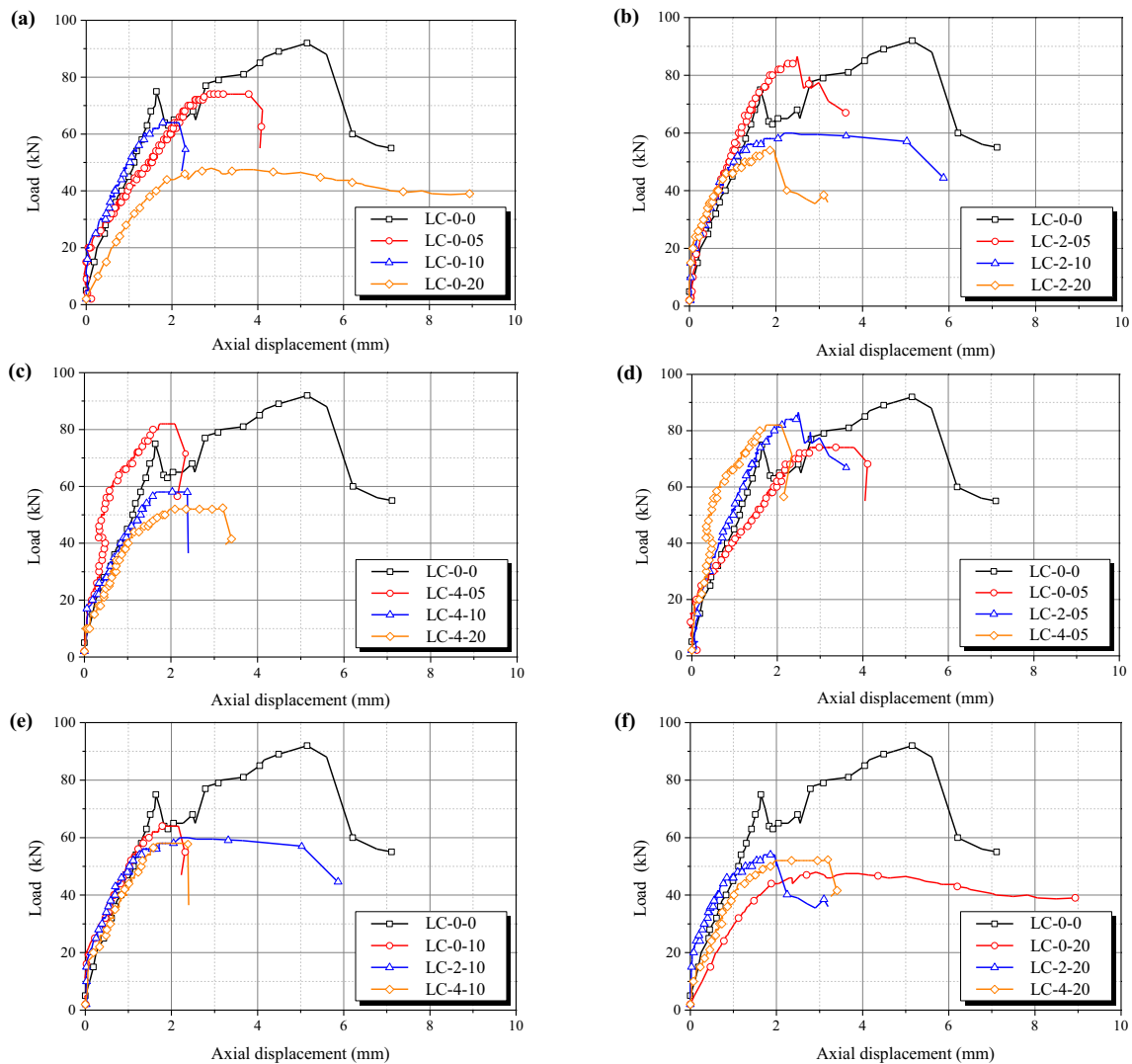**Fig. 9** Load–axial displacement curves of different specimens

3.5 Load–Axial Strain Relationship

The load–axial strain relationship of the specimens is shown in Fig. 10, from which it can be seen that some parts of the specimens are under tension because of the pre-loaded sustained loads. The axial strain of concrete increases as the increase in axial load and the neutral axis gradually moves to the side where the axial load located. The distribution of the axial strain within the cross section indicates that the plane section assumption is still valid. Hence, this assumption can also be used when establishing the model for predicting the ultimate bearing capacity that will be described later in Sect. 4.

The comparisons of the load–axial strain cures of specimens with different corrosion levels show that the bearing capacity of corroded specimens is significantly lower than that of non-corroded one, and under the same

load, the axial strain of corroded specimens is higher than that of non-corroded one. Furthermore, the results demonstrate that the sustained load only has a certain impact on the load–axial strain response. For LC-4-20, which is under high sustained load and corrosion level, the load–axial strain curve shows most of its cross section is under compression, and only a small part of the section under tension. This observation is quite similar to that of small eccentric compression specimens. This is mainly because the spalling of concrete cover also aggravates as the increase in corrosion level. For columns under the sustained load, the transverse tensile strain will be appeared in concrete due to the Poisson's effect. Thus, the concrete cover will partly or completely be peeled off for columns under the dual role of corrosion expansion force and the transverse tensile stress, reducing the distance between the centric position and the cross section, which in turn reduces
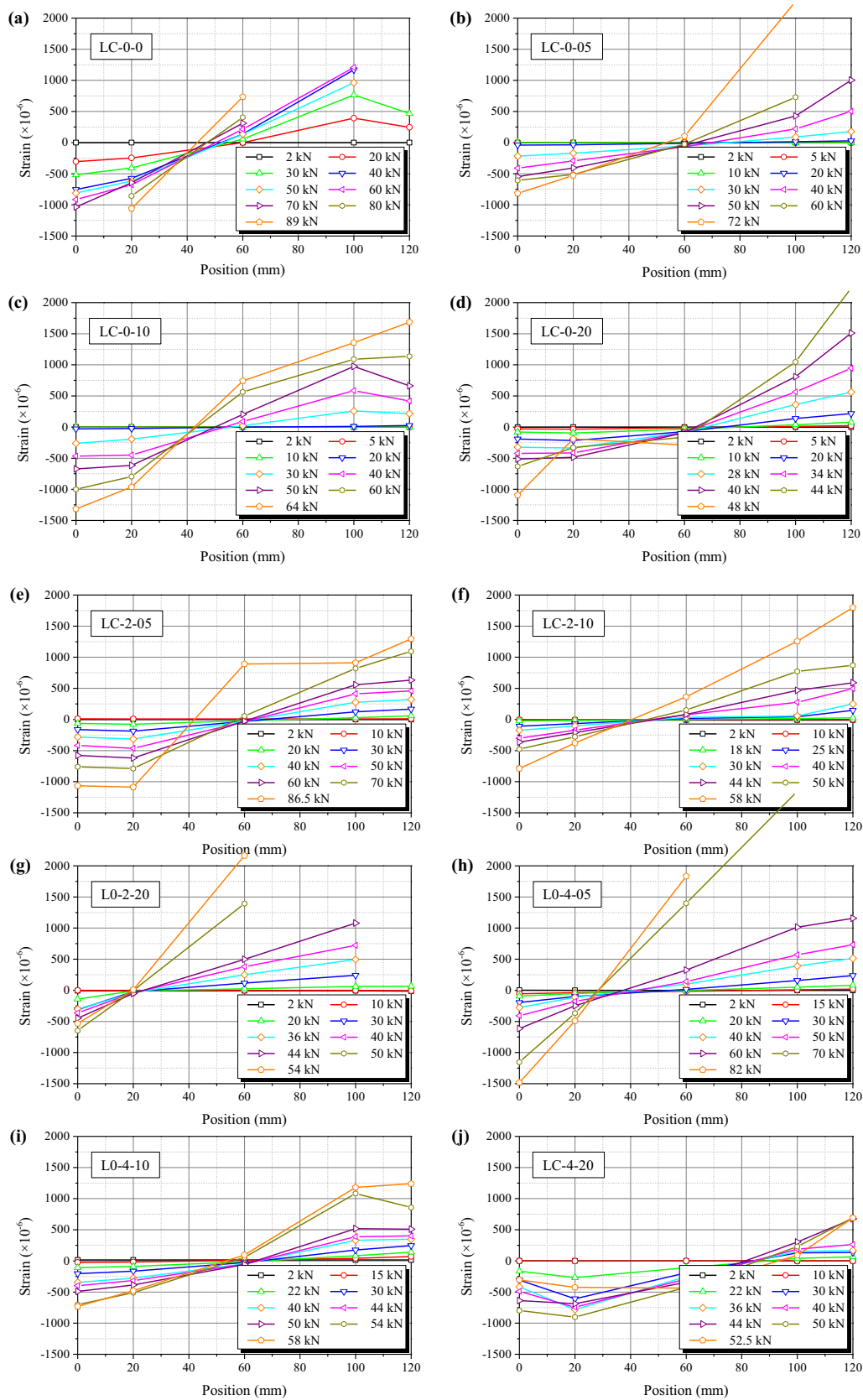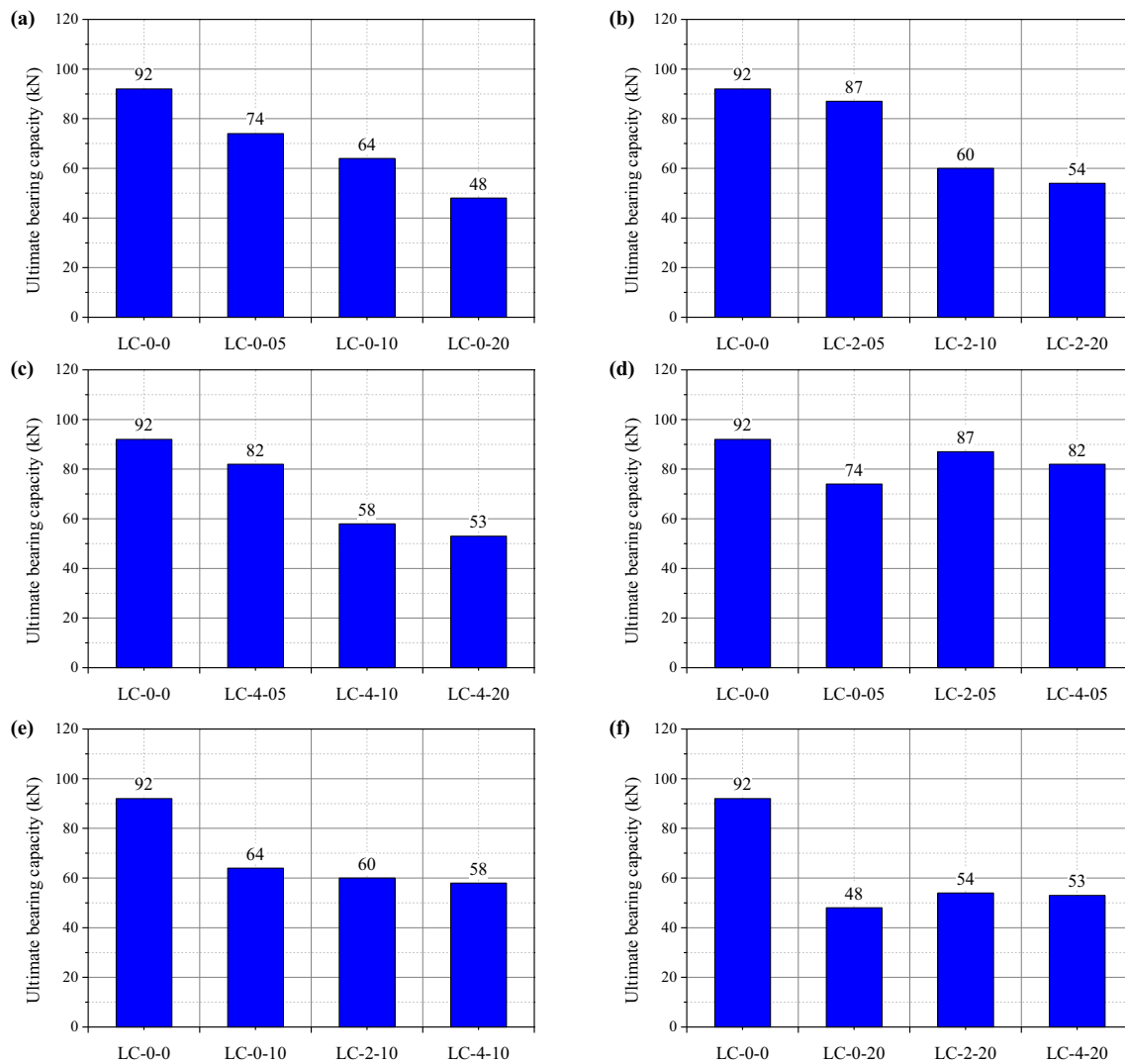
Fig. 10 Load–axial strain curves of specimens

Fig. 11 Effect of reinforcement corrosion level and sustained load on the ultimate bearing capacity of specimens

the eccentricity. In such a case, it is possible to convert the large eccentric specimens to a small eccentric column.

3.6 Ultimate Bearing Capacity

The measured ultimate bearing capacity of specimens is shown in Fig. 11. It can be seen that the ultimate bearing capacity of specimens reduces obviously as the increase in reinforcement corrosion level. Also, a minor reduction is observed when the level of sustained load increases, although occasional increase is also found (e.g., LC-0-20 vs. LC-2-20 or LC-4-20). This is mainly because the large eccentric column is "tensile failure," characterized by the reinforcement away from the axial force first reaches the tensile yielding strength and then the concrete near the side of the axial force is crushed. On the other hand, the tension

side of the large eccentric column can be cracked under minor sustained load, and erosion ions can reach the surface of the steel bar directly. With the above analysis, it is clear that except for some small fluctuations, the coupling effects of reinforcement corrosion and sustained load on the ultimate bearing capacity can be generally observed. Particularly for the specimen L-4-20, a reduction of as much as 42% in terms of the ultimate bearing capacity was found, compared with the control specimen L-0-0.
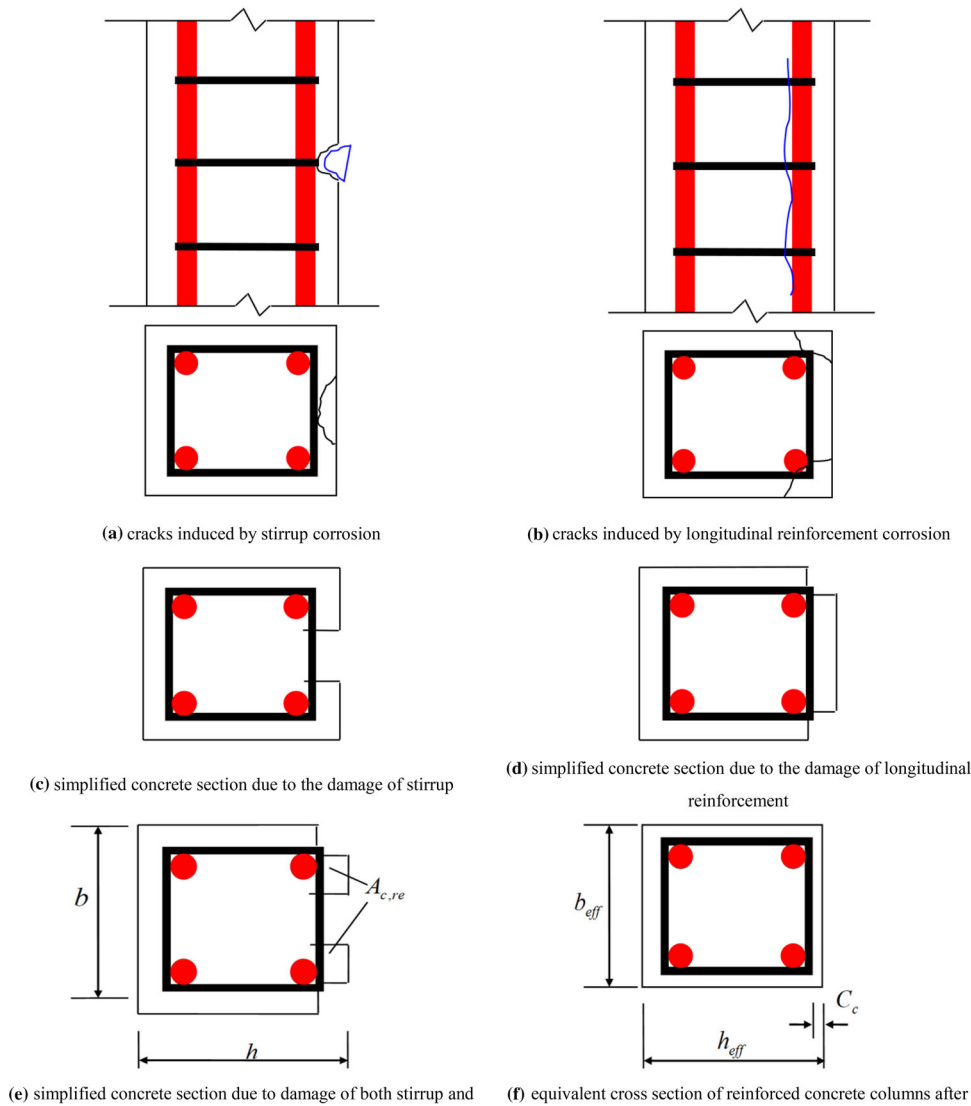
(a) cracks induced by stirrup corrosion

(b) cracks induced by longitudinal reinforcement corrosion

(c) simplified concrete section due to the damage of stirrup

(d) simplified concrete section due to the damage of longitudinal reinforcement

(e) simplified concrete section due to damage of both stirrup and

(f) equivalent cross section of reinforced concrete columns after

Fig. 12 Damage to the concrete due to the corrosion of reinforcements

4 Proposed Model for the Ultimate Bearing Capacity

## 4.1 Coupling Effects of Reinforcement Corrosion and Sustained Load

4.1.1 Loss of Concrete Cross Section

Cracking or spalling of concrete caused by the expansion of reinforcement corrosion induces damage to the concrete section, which not only reduces the effective area of concrete section, but also changes actual section center of the column. Therefore, before evaluating the bearing capacity of the column, the effective cross section of the column should be determined.

Compared with the reinforcement corrosion, the cross section of concrete is easier to be obtained through the

actual measurement. For concrete section, the damage caused by the rust expansion of stirrups corrosion generally is transverse crack or lateral spalling, as shown in Fig. 12a, while the damage caused by rust expansion of reinforcement corrosion generally is longitudinal crack or spalling, as shown in Fig. 12b. Due to the fact that the form of reinforcements in the column is various, and the spalling of concrete is different; thus, the effects of corrosion of longitudinal reinforcements and stirrups on the effective cross section of concrete should be considered, respectively.

For mild steel corrosion when the concrete cover yet is not cracked, the column section takes its original section. If the transverse crack caused by stirrup corrosion and the longitudinal crack caused by longitudinal reinforcement corrosion have been fully developed, the concrete within the scope of crack indeed is out of work. Therefore, the contribution of these cracked parts of concrete should not

(a) RC column with corroded stirrups   **(b)** buckling model of longitudinal compressive reinforcement
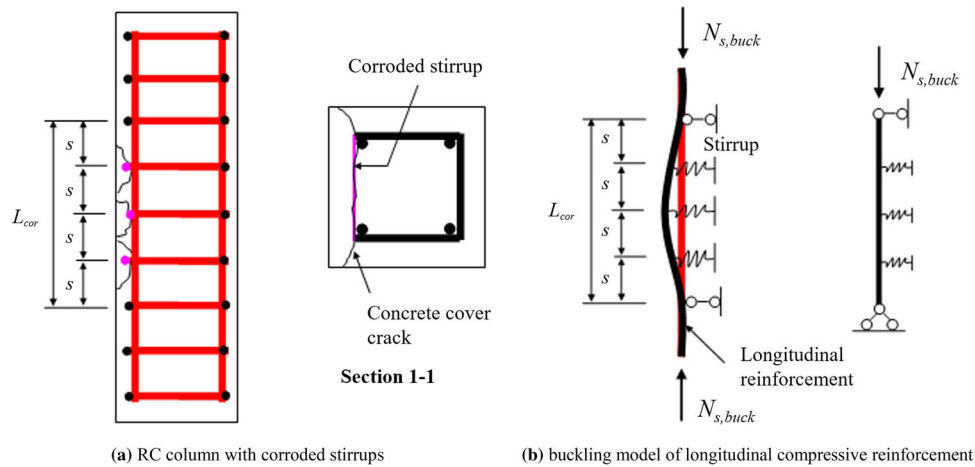
Fig. 13 Deteriorated RC column and mechanical model for buckling of longitudinal reinforcement

be taken into consideration when calculating the ultimate bearing capacity of the column.

The damage caused by the corrosion of stirrups and longitudinal reinforcements in concrete cross section was simplified in the way shown in Fig. 12c, d, respectively, as well as the simplified concrete section considering both of them in Fig. 12e. For axial compression columns, the simplified cross section can be directly used in the calculation. For eccentric compression columns, in order to further simplify the calculation, the final cross section of the column is equivalent to a rectangular termed as $b_{\text{eff}} \times h_{\text{eff}}$. Considering the concrete within the scope of cracks that are out of work, the thickness of concrete cover is C_c, with the method of equivalent area calculated according to Fig. 12e, f, using the following formula,

$$A_{c,re} = C_c \times h_{\text{eff}} \quad \text{or} \quad A_{c,re} = C_c \times b_{\text{eff}}. \tag{1}$$

4.1.2 Reinforcement Corrosion

4.1.2.1 Influence of Stirrup Corrosion on the Constraints of Longitudinal Reinforcement
The concrete column with corroded stirrups is schematically shown in Fig. 13a. Stirrup corrosion not only leads to the cracking and spalling of concrete and reduces its constraints on core concrete core, but also reduces its lateral restraint to longitudinal reinforcement. Thus, premature buckling failure of longitudinal reinforcement may occur before it reaches ultimate strength. The buckling model of the longitudinal compressive bar with stirrup corrosion is established according to the assumption shown in Fig. 13b. The constraint of stirrups to main reinforcement in the section without stirrup corrosion is vertically movable and horizontally immobile hinge constraint. The constraint of the stirrups to the main reinforcement in section with stirrups corrosion is simulated by spring with variable stiffness. The stiffness of the

spring depends on the corrosion level of the stirrups. The formula $P_{\text{critt}} = 3.46 \, (E_r \times J_1 \times k)^{0.5}$ is used to calculate the buckling load of steel reinforcement [32], and such a formula was also used in the literature [33], but the parameter is set to 3.30.

According to the theory of elasticity [34], the buckling bearing capacity of compressive reinforcements with elastic support, as shown in Fig. 13b, is given as follows:

$$N_{s,buck} = 0.6\pi^2 E_s I_s / L_{cor}^2 + 2\sqrt{c_{eq} E_s I_s} \tag{2}$$

where $N_{s,buck}$ is the buckling bearing capacity of the main reinforcement; E_s is the elastic modulus of main reinforcement; I_s is the moment of inertia of the main reinforcement, defined as $I_s = \pi d_s^4/64$; d_s is the diameter of reinforcement; L_{cor} is the stirrup corrosion segment length; $C_{eq} = k_{st}/s$; $k_{st} = E_{st} A_{c,st}/l_{st}$; E_{st} is the elastic modulus of stirrups, which is assumed to be unchanged before and after corrosion; and $A_{c,st}$ is the remaining cross-sectional area after stirrup corrosion, considering the influence of pitting corrosion.

If the calculated buckling capacity is greater than the strength of bearing capacity of longitudinal reinforcement, it means that stirrup has enough constraints on the longitudinal reinforcement, and the strength of longitudinal reinforcement can be fully utilized, indicating that the buckling failure of longitudinal reinforcement does not occur prior to the strength failure.

4.1.2.2 The Mechanical Properties of Corroded Reinforcement
Studies have shown that the corrosion not only causes the section loss of reinforcement, but also leads to the degradation of mechanical properties. The yielding strength, ultimate tensile strength, and elongation decrease as the increase in corrosion level. When the corrosion level is less than 10%, the corroded reinforcement still has an obvious yielding stage, but if the corrosion level is greater

than 20%, the yielding stage can be ignored. The change laws of the nominal yielding strength and the elongation of corroded reinforcement by electrochemical corrosion tests have already been investigated [35]. Based on the results, the nominal yielding strength and the elongation of corroded reinforcement, f_{yc} and ε_{usc}, were determined as:

In the cases of $0 < \rho < 5\%$,

$$f_{yc} = (1 - 1.068\rho)f_y \tag{3}$$

$$\varepsilon_{usc} = (1 - 2.480\rho)\varepsilon_{us} \tag{4}$$

and $\rho > 5\%$,

$$f_{yc} = (0.962 - 0.848\rho)f_y \tag{5}$$

$$\varepsilon_{usc} = (1.088 - 3.573\rho)\varepsilon_{us} \tag{6}$$

where ρ is the average sectional corrosion level of reinforcement; f_y is the yielding strength of non-corroded reinforcement; and ε_{us} is the ultimate strain of non-corroded reinforcement.

4.1.3 Sustained Load

Under the sustained load, the redistribution of stress between the concrete and reinforcements is expected to occur, because of the deformation of concrete. Usually, the stress within the concrete is found to decrease, while the stress within the reinforcements increases accordingly. As such, an additional eccentricity is therefore generated, which leads to a decrease in the ultimate bearing capacity of eccentric columns. To represent this second-order effect, an eccentricity magnifying coefficient η was used in line with the code GB50010-2010 [36],

$$\eta = \frac{e_i + f}{e_i} = 1 + \frac{f}{e_i} \tag{7}$$

where f is the maximum lateral deflection, and e_i is the eccentricity. The deflection of the column at any point y as shown in Fig. 14 can be approximately described as

$$y = f \cdot \sin\frac{\pi x}{l_0}, \tag{8}$$

and the curvature of the deflection curve is given as

$$\varphi = -\frac{d^2 y}{dx^2} = f\left(\frac{\pi}{l_0}\right)^2 \sin\frac{\pi x}{l_0} \tag{9}$$

In the case of $x = l_0/2$ where the maximum lateral deflection is obtained, the corresponding curvature is written as

$$\varphi\big|_{x=\frac{l_0}{2}} = \frac{d^2 y}{dx^2}\bigg|_{x=\frac{l_0}{2}} = f\left(\frac{\pi}{l_0}\right)^2 \tag{10}$$

According to the plane assumption, the curvature can be also determined by the strain within the cross section shown in Fig. 15,

$$\varphi = \frac{\varepsilon_c + \varepsilon_s}{h_0} \tag{11}$$

Taking the deformation of concrete into account, the above expression can be revised as

$$\varphi = \frac{K \cdot \varepsilon_c + \varepsilon_s}{h_0} \tag{12}$$

where K is the correction factor considering the increase in compressive strain due to the concrete creep under long-term load, and it is normally given as $K = 1.25$. Hence, for the section that is in the limit state, i.e., the critical section where the maximum lateral deflection is observed, the corresponding curvature φ_b is written as

$$\varphi_b = \frac{K \cdot \varepsilon_{cu} + \varepsilon_y}{h_0} \tag{13}$$

where ε_{cu} and ε_y are the ultimate strain of concrete and steel reinforcement, respectively, taken as $\varepsilon_{cu} = 0.0033$ and $\varepsilon_y = 0.002$. Upon this, the value of $1/158.1\,h_0$ is therefore figured out for the critical curvature φ_b. Finally, introducing Eq. (13) into Eqs. (7) and (10), the eccentricity magnifying coefficient η is obtained.

As an alternative, for simplicity, an experiment-based empirical equation is also suggested for the estimation of the eccentricity magnifying coefficient η:

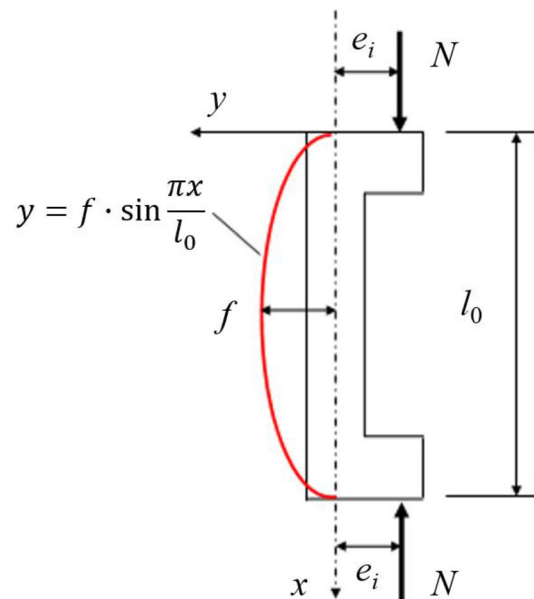$$\eta = 1 + \frac{1}{1300}\frac{h_0}{e_i}\left(\frac{l_0}{h}\right)^2 \xi_c \tag{14}$$

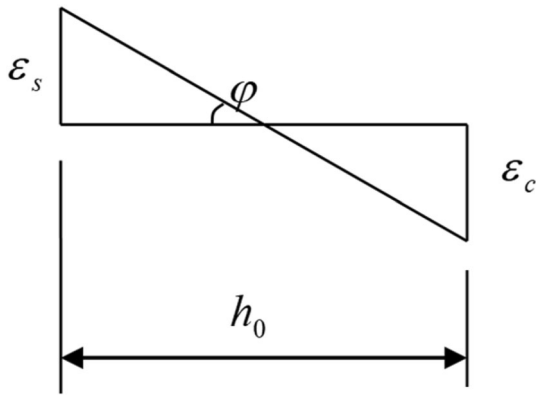**Fig. 14** Lateral deflection of RC column

Fig. 15 Distribution of strain within the cross section

where the coefficient ξ_c is numerically calculated as $\xi_c = 0.2 + 2.7e_i/h_0$. In the case of $\xi_c > 1$, the value of $\xi_c = 1$ is specified.

4.2 Estimation of the Ultimate Bearing Capacity

4.2.1 Basic Assumptions

To establish the analytical model for evaluating the ultimate bearing capacity, the following assumptions are made:

1. The strain distribution along the depth of cross section obeys the plain section assumption.
2. For the corroded reinforcement, according to the results of the literature [37], when the reinforcement corrosion level is smaller than 20%, an obvious yielding platform can be still observed. Therefore, the ideal elastic–plastic model as shown in Fig. 16 was adopted in this study,

$$\sigma_s = \begin{cases} E_s\varepsilon_s & \varepsilon_s \le \varepsilon_{yc} \\ f_{yc} & \varepsilon_s > \varepsilon_{yc} \end{cases} \quad (15)$$

where σ_s and ε_s are the stress and strain of reinforcement, respectively; E_s is the elastic modulus.

3. For the stress–strain relation of the concrete, the widely acknowledged model suggested by [36], as shown in Fig. 17, was adopted as follows:

$$\sigma_c = \begin{cases} f_c\left[1 - (1 - \varepsilon_c/\varepsilon_0)^2\right] & \varepsilon_c \le \varepsilon_0 \\ f_c & \varepsilon_0 < \varepsilon_c < \varepsilon_{cu} \end{cases} \quad (16)$$

where σ_c and ε_c are the stress and strain of concrete, respectively; f_c and ε_0 are the compressive strength and corresponding strain; ε_{cu} is the ultimate compressive strain. In practice, $\varepsilon_0 = 0.002$ and $\varepsilon_{cu} = 0.0033$ are specified. In view of the spalling of concrete, only the contribution from the core concrete is considered,
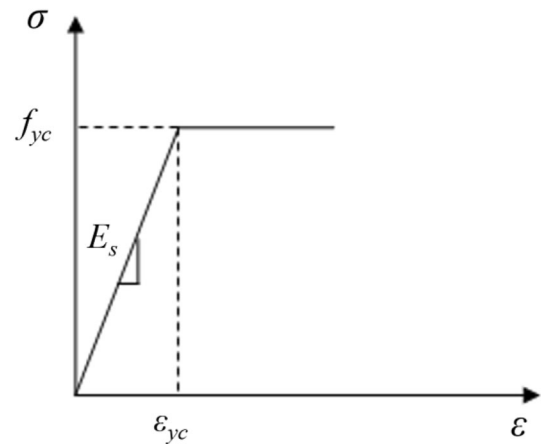

Fig. 16 Stress–strain relation of steel reinforcement

while the contribution of concrete tensile strength is not considered.

4. Within the regions where the stirrups are corroded, the constrains to the longitudinal reinforcements are represented by elastic springs.

4.2.2 Analytical Formulation

Upon the above analyses, the simplified schematic diagram of the stress distribution within the cross section is plotted in Fig. 18.

In accordance with the principles of equilibrium and compatibility, the following equations are always valid,

$$N_u = \alpha_1 f_c b_{eff} x + \sigma'_{sc}A'_{sc} - \sigma_{sc}A_{sc} \quad (17)$$

$$N_u e \le \alpha_1 f_c b_{eff} x \left(h_{0,eff} - \frac{x}{2}\right) + \sigma'_{yc}A'_{sc}\left(h_{0,eff} - a'_s\right) \quad (18)$$
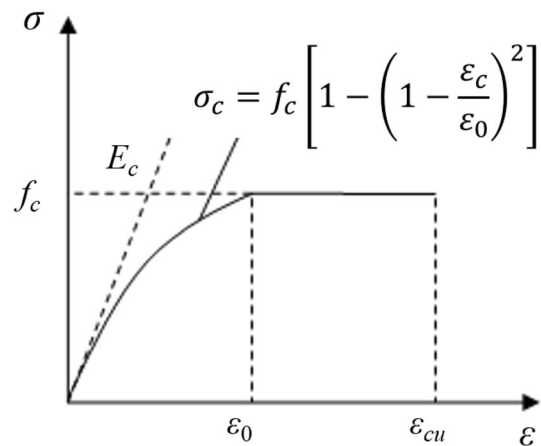
with

Fig. 17 Stress–strain relation of concrete

$$e = \eta e_i + \frac{h}{2} - a_s \tag{19}$$

$$e_i = e_0 + e_a \tag{20}$$

$$\sigma'_{sc} = \min\left(f'_{yc}, f'_{sbc}\right) \tag{21}$$

$$\sigma_{sc} = \min\left(f'_{yc}, f'_{sbc}, \sigma_s\right) \tag{22}$$

where α_1 is the coefficient related to the equivalent compressive stress, which is specified according to the code [36]; b_{eff} and $h_{0,eff}$ are the effective width and height of the cross section, respectively; x is the height of the compression zone; σ_{sc} and σ'_{sc} are the stresses of longitudinal reinforcements that are far from and close to the loading axial, respectively; a_s and σ'_s are the concrete covers of corresponding longitudinal reinforcements; e, e_i, e_0, and e_a are the total eccentricity, initial eccentricity, designed eccentricity, and additional eccentricity generated from the uncertainty of loading position, the inhomogeneity of concrete quality, etc. [38], respectively; η is the eccentricity magnifying coefficient, defined in Eq. (7); f'_{sbc} is the stress when the longitudinal reinforcements fail in a buckling failure, given as

$$f'_{sbc} = \frac{N_{s,buck}}{A'_{sc}} = \frac{0.6\pi^2 E_s I_s}{A'_{sc} L^2_{cor}} + \frac{2\sqrt{c_{eq} E_s I_s}}{A'_{sc}} \tag{23}$$
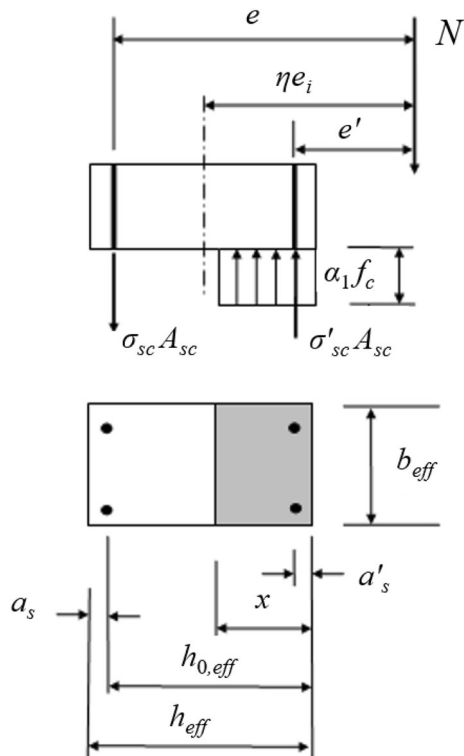

Fig. 18 Simplified schematic diagram of ultimate bearing capacity of an eccentric RC column

and σ_s is the characteristic stress of the reinforcement. If the ratio $\xi = x/h_{0,eff}$ is smaller than the critical value $\xi_b = 0.8/(1 + f_y/E_s\varepsilon_{cu})$, the equation $\sigma_s = f_{yc}$ is assumed. Otherwise, the value of σ_s is given as

1. In the case that the reinforcements far away from the loading are under tension,

$$\sigma_s = E_s\left(\frac{0.8h_{0,eff}}{x0} - 1\right)\varepsilon_{cu} < f_{yc} \tag{24}$$

or these reinforcements are also under compression,

$$\sigma_s = \min\left(E_s\left(\frac{0.8h_{0,eff}}{x0} - 1\right)\varepsilon_{cu}, f'_{sbc}\right) < f_{yc} \tag{25}$$

2. With the above definitions, the ultimate bearing capacity of the specimens can be analytically evaluated, in which the coupling effects of the reinforcement corrosion and the sustained load are taken into consideration.

4.2.3 Validation of the Model

The comparisons between the test results and the analytical results upon respective eccentricity magnifying coefficients in Eqs. (7) and (14) are shown in Table 4. From the table, it can be seen that the ratio between the test results and analytical results ranges from 0.86 to 1.19. The average ratio is 0.995, and the standard deviation is 0.101. The close agreements indicate that the coupling effects of the reinforcement corrosion and the sustained load on the ultimate bearing capacity of specimens are well reflected. The reduction in cross section of both longitudinal reinforcements and stirrups and its adverse effect on the buckling of the main reinforcements, as well as the concrete deformation induced by the sustained load, are reasonably reproduced.

5 Conclusions

Based on the experimental investigation on the mechanical performance of RC columns subjected to reinforcement corrosion and sustained load simultaneously, as well as the analytical prediction of the ultimate bearing capacity of corroded specimens, the following conclusions can be summarized:

1. The failure characteristics, ultimate bearing capacity, and load–axial deformation relationships of the tested specimens clearly indicate that the reinforcement corrosion and sustained load exhibit obvious coupling effects in deteriorating the mechanical performance of columns.

Table 4 Comparison between analytical predictions and test results of specimens

Column	Test results $N_{u,test}$ (kN)	Analytic results (kN)		Ratio between the test results and analytical results	
		$N_{u,1}$ (kN)	$N_{u,2}$ (kN)	$N_{u,1}/N_{u,test}$	$N_{u,2}/N_{u,test}$
LC-0-0	92	83	80	0.90	0.87
LC-0-5	74	70	68	0.95	0.92
LC-0-10	64	69	67	1.08	1.05
LC-0-20	48	52	49	1.08	1.02
LC-2-5	87	78	75	0.90	0.86
LC-2-10	60	67	64	1.12	1.07
LC-2-20	54	57	55	1.06	1.02
LC-4-5	82	78	76	0.95	0.93
LC-4-10	58	69	67	1.19	1.16
LC-4-20	53	52	50	0.98	0.94

The analytical results of $N_{u,1}$ are calculated based on the eccentricity magnifying coefficient shown in Eq. (7), while the analytical results of $N_{u,2}$ are calculated based on the eccentricity magnifying coefficient shown in Eq. (14)

2. The sustained load has an obvious effect on the promotion of the corrosion level of steel reinforcements. The corrosion level increases gradually as the load level increases, and it is more pronounced for the reinforcements on the side far from the sustained load when compared with those close to the load.

3. Compared with the control specimen L-0-0, the ultimate bearing capacity of the specimen L-4-20 reduced as much as about 42%. Besides, the sustained load may enhance the stiffness of eccentric columns, which, however, will obviously make the columns to be much more brittle, resulting in premature failure.

4. The improved model taking the effects of the corrosion of both longitudinal reinforcements and stirrups, as well as the concrete spalling, into consideration can reasonably predict the ultimate bearing capacity of corroded columns subjected to sustained load.

References

1. Darwin D, Dolan CW, Nilson AH (2016) Design of concrete structures. McGraw-Hill, Berlin
2. Qiu F, Li W, Pan P, Qian J (2002) Experimental tests on reinforced concrete columns under biaxial quasi-static loading. Eng Struct 24(4):419–428
3. Rodrigues H, Arêde A, Varum H, Costa AG (2013) Experimental evaluation of rectangular reinforced concrete column behaviour under biaxial cyclic loading. Earthq Eng Struct Dynam 42(2):239–259
4. Parvin A, Wang W (2001) Behavior of FRP jacketed concrete columns under eccentric loading. J Compos Constr 5(3):146–152
5. Torres-Acosta AA, Martínez-Madrid M (2003) Residual life of corroding reinforced concrete structures in marine environment. J Mater Civ Eng 15(4):344–353
6. Dhakal RP, Maekawa K (2002) Reinforcement stability and fracture of cover concrete in reinforced concrete members. J Struct Eng 128(10):1253–1262
7. Bažant ZP, Kwon YW (1994) Failure of slender and stocky reinforced concrete columns: tests of size effect. Mater Struct 27(2):79–90
8. Huang L, Xu L, Chi Y, Xu H (2015) Experimental investigation on the seismic performance of steel-polypropylene hybrid fiber reinforced concrete columns. Constr Build Mater 87:16–27
9. Boumarafi A, Abouzied A, Masmoudi R (2015) Harsh environments effects on the axial behaviour of circular concrete-filled fibre reinforced-polymer (FRP) tubes. Compos B Eng 83:81–87
10. Prachasaree W, Limkatanyu S, Wangapisit O, Kraidam S (2018) Field investigation of service performance of concrete bridges exposed to tropical marine environment. Int J Civ Eng 16(12):1757–1769
11. Ma Y, Che Y, Gong J (2012) Behavior of corrosion damaged circular reinforced concrete columns under cyclic loading. Constr Build Mater 29:548–556
12. Choe DE, Gardoni P, Rosowsky D, Haukaas T (2009) Seismic fragility estimates for reinforced concrete bridges subject to corrosion. Struct Saf 31(4):275–283
13. Lee HS, Kage T, Noguchi T, Tomosawa F (2003) An experimental study on the retrofitting effects of reinforced concrete columns damaged by rebar corrosion strengthened with carbon fiber sheets. Cem Concr Res 33(4):563–570
14. Tapan M, Aboutaha RS (2011) Effect of steel corrosion and loss of concrete cover on strength of deteriorated RC columns. Constr Build Mater 25(5):2596–2603
15. Tapan M, Aboutaha RS (2008) Strength evaluation of deteriorated RC bridge columns. J Bridge Eng 13(3):226–236
16. Wang XH, Liang FY (2008) Performance of RC columns with partial length corrosion. Nucl Eng Des 238(12):3194–3202
17. Asghshahr MS, Rahai A (2018) Seismic assessment of reinforced concrete bridge under chloride-induced corrosion. Int J Civ Eng 16(6):681–693
18. Kumar R, Gardoni P, Sanchez-Silva M (2009) Effect of cumulative seismic damage and corrosion on the life-cycle cost of

reinforced concrete bridges. Earthq Eng Struct Dynam 38(7):887–905

19. Soylev TA, François R (2003) Quality of steel–concrete interface and corrosion of reinforcing steel. Cem Concr Res 33(9):1407–1415

20. Torres-Acosta AA, Navarro-Gutierrez S, Terán-Guillén J (2007) Residual flexure capacity of corroded reinforced concrete beams. Eng Struct 29(6):1145–1152

21. Bentur A, Berke N, Diamond S (1997) Steel corrosion in concrete: fundamentals and civil engineering practice. CRC Press, Boca Raton

22. Ye H, Fu C, Jin N, Jin X (2018) Performance of reinforced concrete beams corroded under sustained service loads: a comparative study of two accelerated corrosion techniques. Constr Build Mater 162:286–297

23. Li H, Li B, Jin R, Li S, Yu JG (2018) Effects of sustained loading and corrosion on the performance of reinforced concrete beams. Constr Build Mater 169:179–187

24. Hou C, Han LH, Zhao XL (2013) Full-range analysis on square CFST stub columns and beams under loading and chloride corrosion. Thin Walled Struct 68:50–64

25. Guo A, Li H, Ba X, Guan X, Li H (2015) Experimental investigation on the cyclic performance of reinforced concrete piers with chloride-induced corrosion in marine environment. Eng Struct 105:1–11

26. Yin SP, Hu XQ, Hua YT (2018) Study on the compression performance of small eccentric degradation columns strengthened with TRC in a chloride environment. Constr Build Mater 176:50–59

27. Green MF, Bisby LA, Fam AZ, Kodur VK (2006) FRP confined concrete columns: behaviour under extreme conditions. Cement Concr Compos 28(10):928–937

28. Xu S, Li A, Ji Z, Wang Y (2016) Seismic performance of reinforced concrete columns after freeze–thaw cycles. Constr Build Mater 102:861–871

29. Bouteiller V, Cherrier JF, L'Hostis V, Rebolledo N, Andrade C, Marie-Victoire E (2012) Influence of humidity and temperature on the corrosion of reinforced concrete prisms. Eur J Environ Civ Eng 16(3–4):471–480

30. Ministry of Housing and Urban-Rural Development of the People's Republic of China (2011) JGJ/T 55–2011: specification for mix proportion design of ordinary concrete

31. China Academy of Building Research (2002) GB/T 50082-2009: standard for test methods of long-term performance and durability of ordinary concrete

32. Campione Giuseppe, Minafò Giovanni (2010) Compressive behavior of short high-strength concrete columns. Eng Struct 32:2755–2766

33. Sato Y, Ko H (2008) Modeling of reinforcement buckling in RC columns confined with FRP. J Adv Concr Technol 6(1):195–204

34. Chen WK (2018) Stability design of steel frames. CRC Press, Boca Raton

35. Zhang W, Song X, Gu X, Li S (2012) Tensile and fatigue behavior of corroded rebars. Constr Build Mater 34:409–417

36. Ministry of Housing and Urban-Rural Development of the People's Republic of China (2010) GB 50010-2010: code for design of concrete structures

37. Almusallam AA (2001) Effect of degree of corrosion on the properties of reinforcing steel bars. Constr Build Mater 15(8):361–368

38. Claeson C, Gylltoft K (1998) Slender high-strength concrete columns subjected to eccentric loading. J Struct Eng 124(3):233–240